Commissioning of Laser Electron Gamma Beamline SLEGS at SSRF

Hong-Wei Wang(王宏伟)[a,b,c,①], Gong-Tao Fan(范功涛)[a,b,c,②], Long-xiang Liu(刘龙祥)[a,b], Hang-hua Xu(许杭华)[a,b], Wen-Qing Shen(沈文庆)[a,b,c], Yu-gang Ma(马余刚)[b,d,f], Hiroaki Utsunomiya(宇都宮弘章)[a,e], Long-Long Song(宋龙龙)[a], Xi-Guang Cao(曹喜光)[a,b,c], Zi-Rui Hao(郝子锐)[b,c], Kai-jie Chen(陈开杰)[b,f] , Sheng Jin(金晟)[b,c], Yu-Xuan Yang(杨宇萱)[b,g], Xin-Rong Hu(胡新荣)[b,c], Xin-Xiang Li(李鑫祥)[b,c], Pan Kuang(匡攀)[b,c]

a Shanghai Advanced Research Institute, Chinese Academy of Sciences, Shanghai 201210, China
b Shanghai Institute of Applied Physics, Chinese Academy of Sciences, Shanghai 201800, China
c University of Chinese Academy of Science, Beijing 100049, China
d Fudan University, Shanghai 200433, China
e Department of Physics, Konan University, Kobe 658-8501, Japan
f ShanghaiTech University, Shanghai 201210, China
g Zhengzhou University, Henan 450001, China

Abstract

Shanghai Laser Electron Gamma Source (SLEGS) is a powerful gamma source to provide MeV gamma-ray beams for nuclear science and technology. It is developed as one of the sixteen beamline stations in Phase II Project of the Shanghai Synchrotron Radiation Facility (SSRF). The slant-scattering mode is for the first time systematically employed in the laser Compton scattering (LCS) at SLEGS to produce energy-tunable quasi-monoenergetic gamma-ray beams. SLEGS officially completed its commissioning from July to December 2021. Gamma-rays in energy range of 0.25 - 21.7 MeV with the flux of 2.1×10^4 - 1.2×10^7 photons/s and the energy spread of 2 – 15 % are produced during the test. This paper reports results of the commissioning of the SLEGS beamline.

Keywords

SLEGS, Laser Compton Scattering, Slant-scattering Mode, Back-scattering Mode

1 Introduction

The photonuclear reaction forms a unique field of nuclear physics and astrophysics for the well-known electromagnetic interaction. As early as 1960s through 1980s, the systematic study of the isovector giant-dipole resonance was carried out in photoneutron cross section measurements throughout the chart of nuclei in Saclay Laboratory, France, and Lawrence Livermore National Laboratory (LLNL), USA, with the positron in-flight annihilation technology. However, a large discrepancy between the Saclay and LLNL data of photoneutron cross sections had persisted [1-5], leading to the IAEA project of creating the IAEA photonuclear data library 2019 which includes new data to resolve the long-standing discrepancy [3].

The Laser Compton Scattering (LCS) gamma source has been developed based on the inverse

This work was supported by the National Natural Science Foundation of China (Nos. 11875311, No. 11905274, No. 12005280) and the Chinese Academy of Sciences President's International Fellowship Initiative, Grant No. 2021VMA0025.

① Corresponding author: wanghongwei@zjlab.org.cn,

② Corresponding author: fangongtao@zjlab.org.cn

Compton scattering of laser photons on relativistic electrons in the storage ring. It is the most advanced quasi-monoenergetic gamma-ray source at present which provides a new research opportunity to study photonuclear physics. After 1980s, the TERAS LCS beamline [6] of the National Institute of Advanced Industrial Science Technology (AIST) and the NewSUBARU BL01 LCS beamline of the University of Hyogo, both in Japan [7], and the High Intensity Gamma Source (HIγS) of the Triangle University Nuclear Laboratory (TUNL) in USA, were built for the study of nuclear physics [8]. The high-energy Laser Electron Gamma Source (LEGS) in Stanford Linear Accelerator Center (SLAC) [9] and the Laser Electron Photon beamline (LEPS/LEPS2) at SPRing-8 are dedicated to hadron physics [10]. The TERAS LCS beamline was closed in 2013, while after the installation of a new injection linac, the operation of the NewSUBARU LCS beamline is, at present, limited to industrial applications. Currently, only the high-energy LPES/LEPS2 and the low-energy HIγS are in operation as a major facility. The laser electron gamma source VEGA system in the Extreme Light Infrastructure-Nuclear Physics (ELI-NP) was redesigned in 2019, currently under construction, and is scheduled to run in 2023 [11].

Shanghai Laser Electron Gamma Source (SLEGS) was first proposed in 1998 at the Shanghai Synchrotron Radiation Facility (SSRF). After nearly 20 years of the feasibility study and proto-type development [12-19], it was approved in 2016 as one of the sixteen beamlines in the Phase II project of the SSRF by the National Development and Reform Commission, People's Republic of China. The construction of the SLEGS beamline began in October 2019 and ended in December 2021. The beamline has passed the commissioning test in 2021 and is open to users by the end of 2022 [20].

Using a CO_2 laser with the wavelength of 10.64 μm and the maximum power of 100 W, high-intensity gamma-ray beams are generated in collisions with 3.5 GeV electrons in the SSRF storage ring. SLEGS is designed to operate in two operating modes: One is the laser Compton back-scattering mode at 180˚, which is commonly used worldwide to achieve the highest energy and polarization of gamma-ray beams; The other is the laser Compton slant-scattering mode which enables one to tune the energy of gamma-ray beams by changing the collision angle between the laser and electron beams in the wide range from 160º to 20º.

The slant-scattering is a key technology to produce energy-tunable gamma-ray beams at synchrotron radiation facilities operated at a fixed electron-beam energy. In the past decade, the SINAP-II [15-19] and UVSOR-II have played the pioneering role in the technical development of the slant-scattering. While the UVSOR-II has succeeded in producing MeV gamma-rays at the limited slant-scattering angles of 70º - 110º [21,22], the gamma-ray beam production at SLEGS is systematically carried out in an innovative manner with the dedicated interaction chamber [23] and double collimator system [24,25].

2. Research in SLEGS

SLEGS is designed to generate gamma-ray beams at energies ranging from 0.25 MeV to 21.1 MeV in the slant-scattering at 20°- 160° and at the maximum energy of 21.7 MeV in the back-scattering at 180°. The full-spectrum flux ranges from ~ 10^5 photons/s at 20° to ~ 10^7 at 180º. The 2 % energy resolution is achieved with the 1 - 2 mm collimator which confines the emission angle of the gamma-ray beam less than 0.5 mrad.

The SLEGS serves as a multi-functional experimental platform for research in nuclear science and technology [20]. The research spectrum in basic research, on the one hand, ranges from

collective excitation of nuclei, nuclear equation of state, origin of elements, to ultra-high energy cosmic rays, while that in the application research, on the other hand, ranges from atomic energy, nuclear transmutation, gamma imaging, to national security.

3. SLEGS beamline

The SLEGS beamline is equipped with the following four main components as illustrated in Fig. 1. SLEGS is located in BL03SSID of the SSRF experimental hall. A 3D drawing is shown in Fig. 2.

(1) 100 W CO_2 laser [26] and laser transport.

(2) Interaction chamber for the slant-scattering and multi-function chamber for the back-scattering .

(3) Two-stage coarse and fine collimator and gamma flux attenuator.

(4) Experimental hutch, experimental detector, gamma absorber and data acquisition system

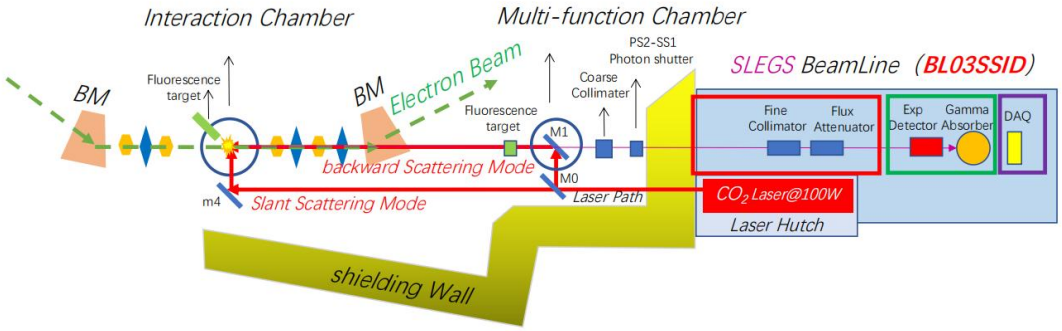

Fig.1 Schematic layout of the SLEGS beamline

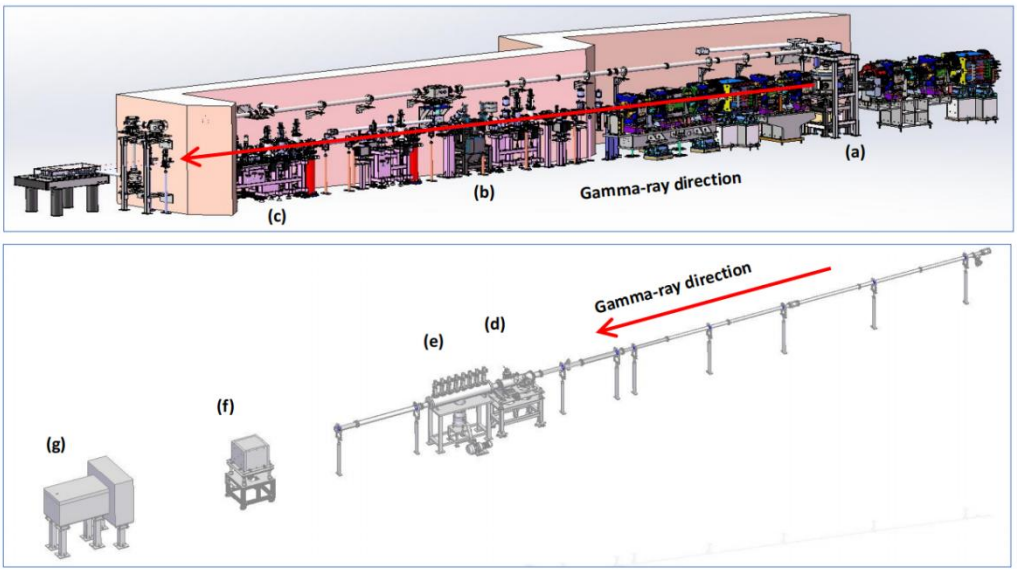

Fig. 2 3D drawing of the SLEGS beamline

(Up: The interaction chamber (a), multi-function chamber (b), and coarse collimator (c) inside the SSRF vault,

Down: The fine collimator (d), flux attenuator (e), experimental detector (f), and gamma absorber

(g) in the SLEGS beamline)

3.1 Laser transport and gamma production

The continuous-wave CO_2 laser of 10.64 μm in wave length and 100 W in laser power is placed in the laser hutch located adjacent to the SSRF vault. The hutch is designed as a clean room for a stable operation of the laser. The CO_2 laser can also be operated in a pulse mode with adjustable laser interval and pulse width, for example, 1 ms laser Interval and 100 μs pulse width at 10 W with a 10 % duty cycle.

The collision between the 10.64 μm laser photons and 3.5 GeV electrons occurs inside the interaction chamber shown in Fig.3 in two collision modes: laser Compton back-scattering and slant-scattering. The CO_2 laser beam goes through the multi-function chamber with the ZnSe window, bends by 90° through a water-cooled mirror and undergoes the head-on collision in the back-scattering mode. In contrast, the laser beam vertically enters into the interaction chamber, passes through the optical elements (the mirrors m_4, m_3, m_2, and m_1 and convex lens f_1 in Fig.3), and horizontally collides with the electron beam in the slant-scattering. The CO_2 laser is finally refocused and led to the beam absorber G through the mirror m_0 and convex lens f_0. The optical elements are mounted on the rotating bracket so that the collision angle between the laser and electron beams are changed from 20° to 160° through the safety stop angle at 90° [23].

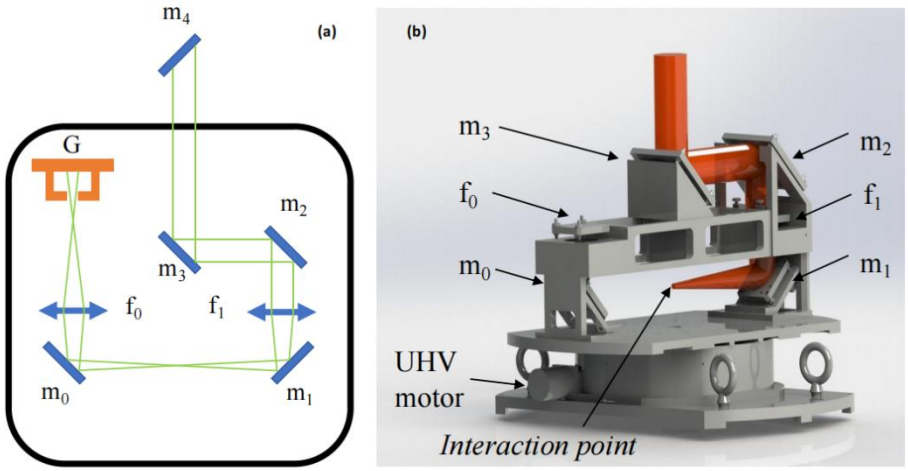

Fig. 3 Schematic picture of configuration of the optical elements (a) and the rotating bracket (b)

3.2 Coarse and fine Collimators

The energy spread and spot size of gamma-ray beams at the target position are determined by the two-stage coarse and fine collimator system, as shown in Fig.4(a) and 4(b). The coarse collimator of a revolver type is made of 300 mm thick lead(Pb), located at ~18 m away from the gamma production point inside the interaction chamber and separated from the high-vacuum SSRF with a 150 μm beryllium(Be) window. It has 10 fixed holes with apertures of 0, 1, 2, 3, 4, 5, 8, 10, 20 and 30 mm. The fine collimator of a camera-shutter type, which is located at 36 m away from the gamma production point in the optical hutch, consists of four sets of shielding shutters, each made of 50 mm tungsten-copper alloy (W 80 % + Cu 20 %). The first and second two sets of the shutters are relatively rotated around the beam axis by 30°, shaping the beam spot into a regular dodecagon [24,25]. The aperture of the fine collimator is changed from 0 mm to 40 mm continuously.

3.3 Flux attenuator

The flux of gamma-ray beams is regulated by the attenuator consisting of 8 pieces oxygen-free copper blocks of the diameter of 50 mm, the thickness of 200 mm, 100 mm (3 pieces), 50 mm (2 pieces), 25 mm and 15 mm, and total thickness of 640 mm, as shown in Fig.4(c). Localized shielding around the fine collimator and flux attenuator are shown in Fig 4(d).

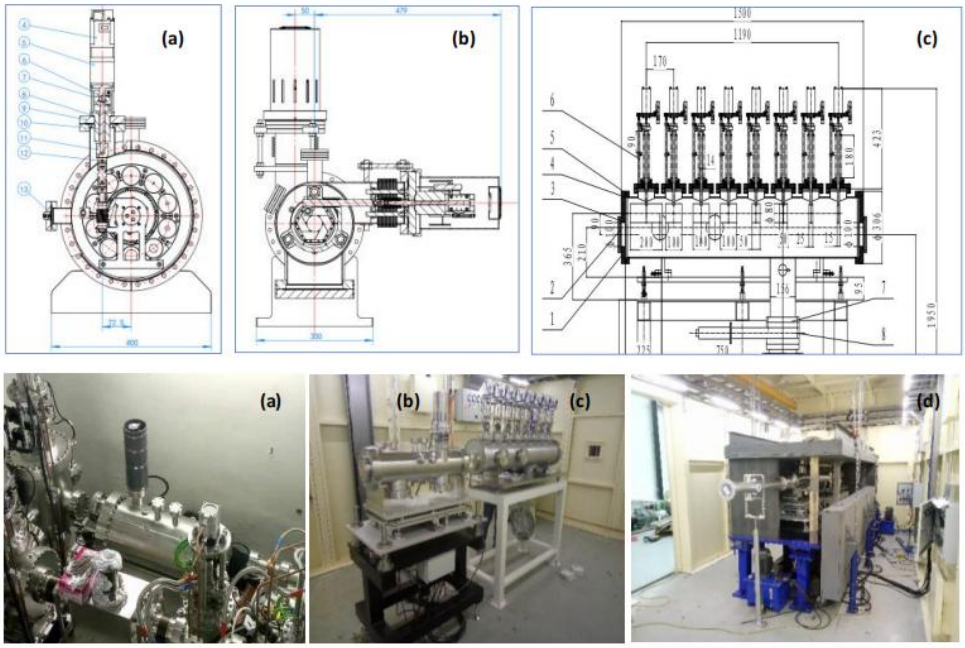

Fig. 4 CAD Drawings (up) and photographs (down) of the SLEGS coarse collimator (a), fine collimator (b), flux attenuator (c) and localized shielding (d).

3.4 Control system

Figures 5(a) and 5(b) show the interface display to remotely control the coarse and fine collimators, respectively. One of the 10 apertures of the coarse collimator is selected and the aperture of the fine collimator is continuously set up in the range of 0 - 40 mm. The horizontal and vertical positions of the coarse and fine collimators are adjusted with the 0.1 mm precision. Fig. 5(c) shows the interface display for selecting any combination of the flux attenuator blocks. The movement of the 200 mm and 100 mm blocks of flux attenuator is monitored with the CCD camera. Figure 5(d) shows the control display of the laser system to be tuned for the laser Compton back and slant-scatterings. The operation condition of the CO_2 laser in the pulse modes is shown in the monitor display, including the pulse interval and width.

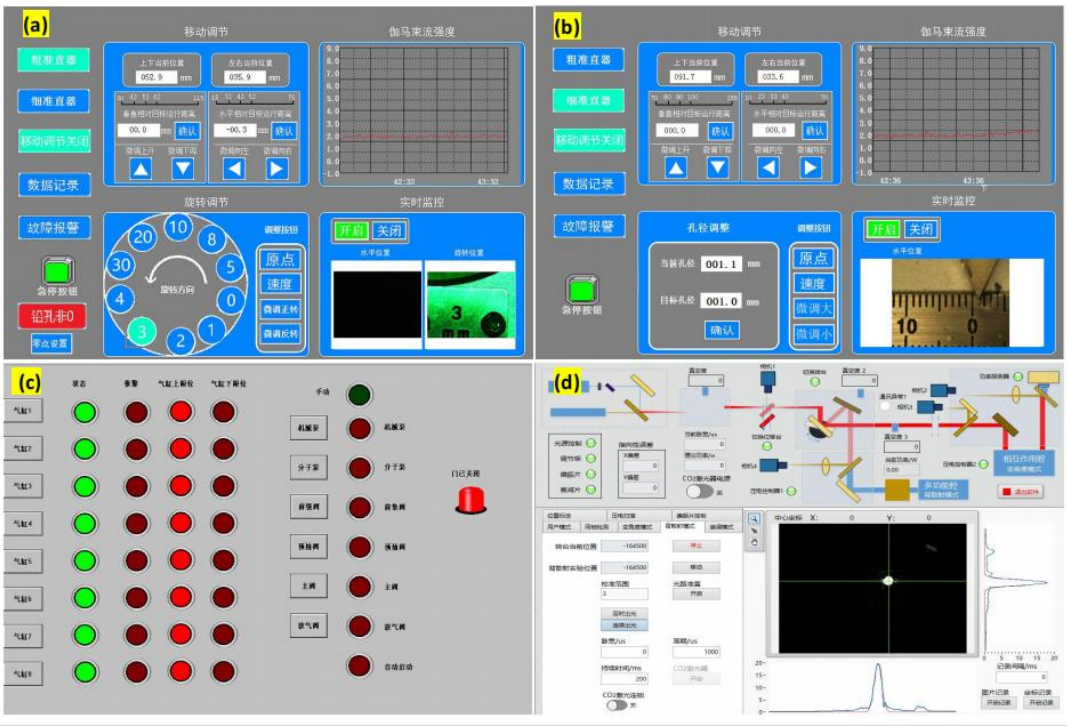

Fig.5 Interface displays of the coarse collimator(a) and fine collimators(b) , flux attenuator (c) and CO_2 laser (d)

4. Commissioning of the SLEGS beamline

Measurements of gamma-ray beams in the commissioning of the SLEGS beamline were performed in the experimental hutch. At the end of the beamline, the unreacted gamma rays enter the gamma absorber made of thick concrete, lead, and high-density polyethylene, as shown in Fig. 1.

4.1 Collimator alignment

The collimators need to be aligned with respect to the gamma-ray beam axis. The collimator alignment was carried out horizontally and vertically by maximizing the intensity of gamma-rays that passed through the collimator. Figures 6(a) and 6(b) show the gamma-ray intensity as a function of vertical and horizontal position of the coarse collimator, respectively. In this collimator position scan, the coarse collimator with the aperture of 2 mm was used along with the 20 mm fine collimator and the 100 mm flux attenuator. A Φ3” x 4”(Φ76.2 mm x 101.6 mm) $LaBr_3$(Ce) detector[27] was used to measure gamma rays. The optimized position of the coarse collimator was found at (51.97 ± 0.04) mm vertically and (34.54 ± 0.03) mm horizontally. The laser - electron collision position and fine collimator also have the same adjustment process.

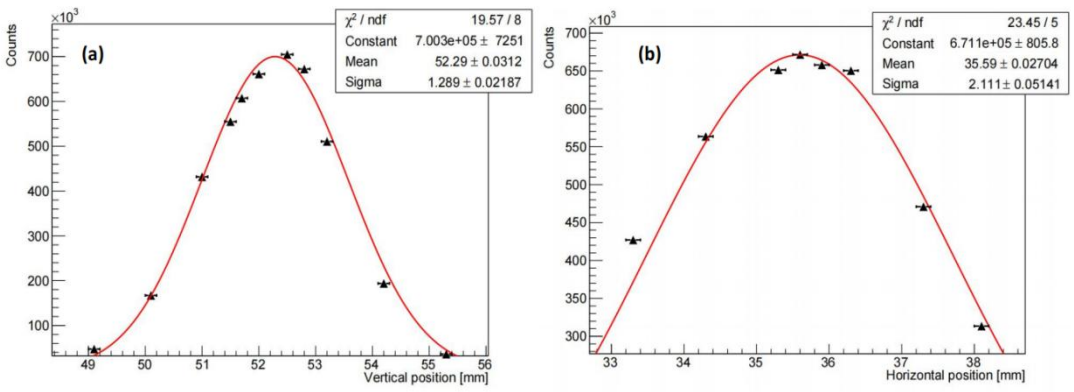

Fig.6 Results of the vertical (a) and horizontal (b) scans of the coarse collimator

4.2 Gamma-ray beam spot

The SLEGS beamline is equipped with two beam spot monitors in the experimental hutch (Fig.7), an X-ray camera called MiniPIX [28] shown in Fig. 7(b) and the Gamma Spot Monitor (GSM) shown in Fig. 7(d). The MiniPIX consists of 256 x 256 silicon pixels with each pixel size of 55 μm x 55 μm and the silicon wafer thickness of 500 μm. The GSM involves an LYSO scintillator of 70 mm in diameter and 2.5 mm in thickness, and collects the scintillation light generated by X and gamma-rays with a CCD/CMOS camera through a 45-degree plane mirror, also designed a 135° optical path as a reserved monitoring channel.

Figure 7(a) shows an example of a beam spot of the bremsstrahlung background measured with MiniPIX. Figure 7(c) shows an example of the gamma-beam spot measured with GSM after subtracting the bremsstrahlung background along with the horizontal (X) and vertical (Y) distributions. The gamma beam spot size in the full width of tenth maximum (FWTM) is horizontally 17.31 mm and vertically 8.91 mm. Since the GSM is placed at about 38 m from the gamma production point, so the gamma-ray emission angles calculated are 0.46 mrad in X and 0.25 mrad in Y.

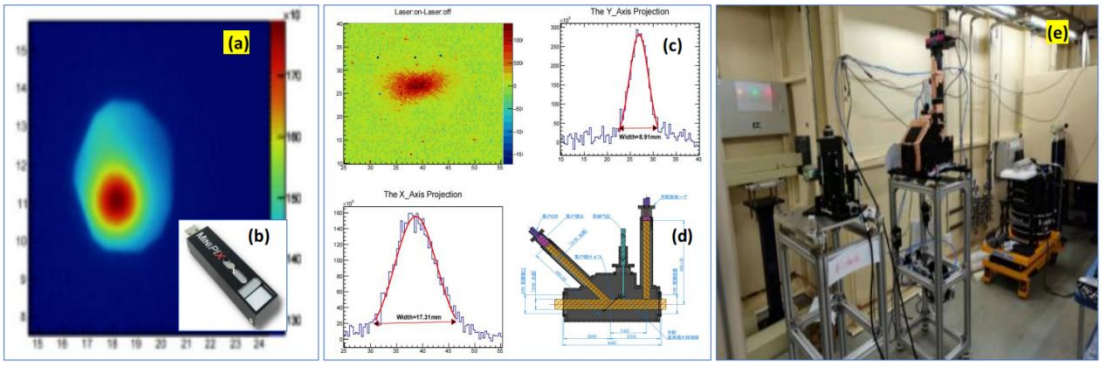

Fig. 7 Bremsstrahlung beam spot (a) and MiniPIX (b) inset, gamma beam spot (b) and GSM (c) inset, the piuture of MiniPIX and GSM (e) in experimental hutch.

4.3 Energy-profile and flux of gamma-ray beams

A Saint-Gobain lanthanum bromide ($LaBr_3(Ce)$) detector of 3”(76.2 mm) in diameter and 4” (101.6 mm) in length with the better energy resolution about ~3 % at 661 keV [27], was used as the energy-profile and flux monitor detector in the commissioning run. The BGO detector of 76.2

mm in diameter and 200 mm in length from SICCAS [29] located in the gamma absorber was used to monitor the gamma flux. The flux value was fed back to the control system of the collimator and laser for online recording and display, and be used as automatic correction of laser power output in future. Figure 8(a) shows a typical response function of the $LaBr_3$(Ce) detector to the gamma-ray beam, where the 3 mm coarse collimator, 3 mm fine collimator, and 1 mm additional lead external collimator were used, but without the flux attenuator. The background gamma spectrum is shown by the green line, where the lower-energy synchrotron radiation and higher-energy bremsstrahlung are seen as well as the internal radiation from ^{138}La in the $LaBr_3$(Ce) detector. Figure 8(b) shows background-subtracted spectra measured at 20°, 90° and 180°.

We have more systematically measured response functions of the $LaBr_3$(Ce) detector to gamma-ray beams produced in the slant-scattering. The background-subtracted spectra are shown in Fig.9. The gamma-ray energy follows the kinematics of the laser Compton slant scattering. The production of gamma-ray beams be confirmed in the energy range of 0.25 - 21.1 MeV in the slant-scattering from 20° to 160° and at 21.7 MeV in the back-scattering at 180°.

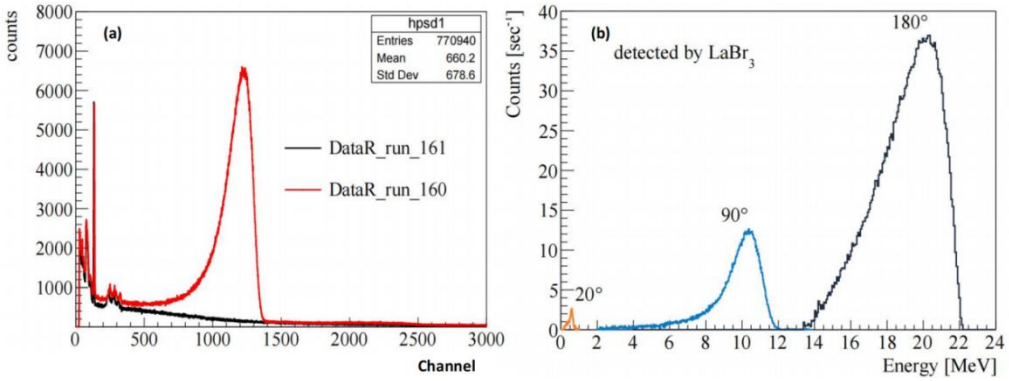

Fig. 8 A typical response function of the $LaBr_3$(Ce) detector to a gamma-ray beam (a) and background-subtracted spectra at 20°, 90° and 180° (b).

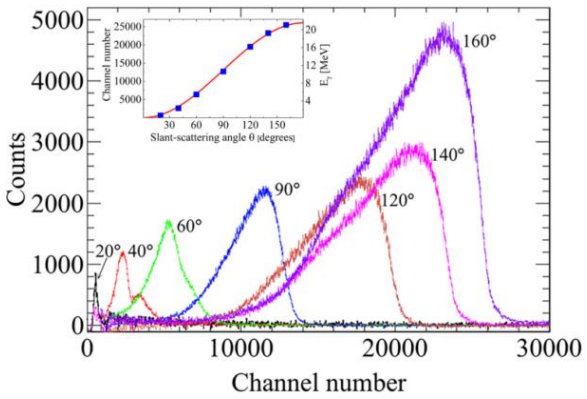

Fig. 9 Response functions of the $LaBr_3$(Ce) detector to gamma-ray beams produced in the slant-scattering and background gamma rays be subtracted. The inset is a comparison of the angle and energy measurements with the theoretically calculated curves

The total gamma-ray flux is an important quantity in the commissioning of the SLEGS

beamline. The required gamma flux to be approved is the total flux at the gamma production point integrated over the whole gamma energy spectrum for the electron beam current I_e = 300 mA(design value). The background-free gamma-ray flux ϕ were measured with the $LaBr_3$(Ce) detector at I_e = 200 mA(test value). After normalizing the measured flux ϕ by $F=\phi/[\eta_D \times \eta_A \times \eta_C] \times$ [300 mA/200 mA] with the detection efficiency η_D of the $LaBr_3$(Ce) detector, the transmission rate η_A of the attenuator, and the tramsmission rate η_C of the collimator hole, the total flux is shown in Fig. 10. The maximum flux at 300 mA electron current and 100 W laser power can reach to about 10^5 photons/s at 20˚ and 10^8 photons/s at 180°.

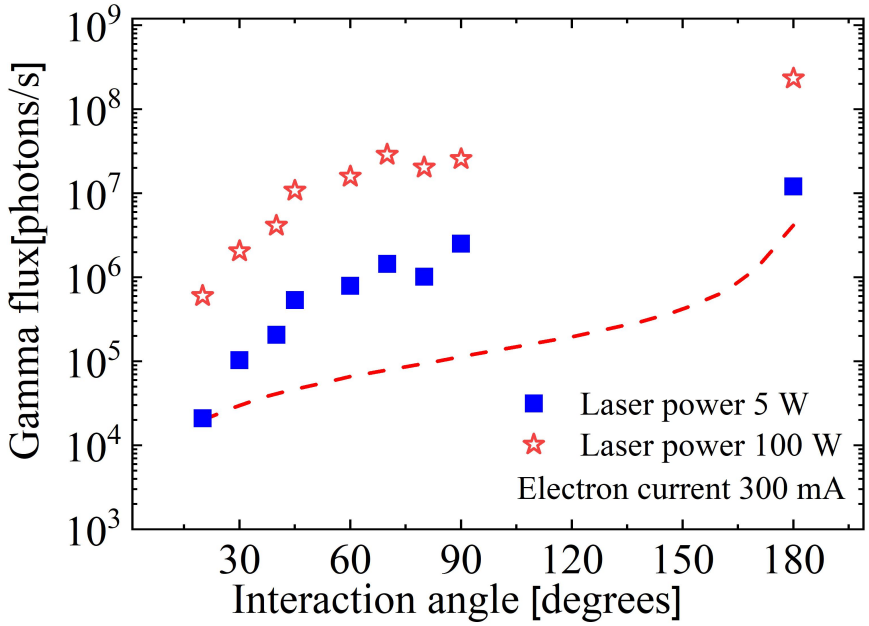

Fig. 10 The total gamma flux at the production point. The red dotted line is the theoretical calculated value at 5 W laser and 300 mA electron current.

4.4 Energy distribution of gamma-ray beams

The electron beam energy of the SSRF storage ring is 3.5 GeV. Because of this high electron-beam energy, the energy of gamma-ray beams produced in the laser Compton scattering strongly depends on the emission angle. Thus, the energy spread (resolution) of the gamma-ray beam is highly sensitive to the angular acceptance defined by the collimator aperture. The black line of Fig. 11 shows the experimental response function of the $LaBr_3$(Ce) detector to gamma rays produced in the back-scattering at 180°. Assuming that the energy distribution of the gamma-ray beam incident on the detector is given by a truncated Breit-Wigner function which is shown by the blue line, we made a Geant4 simulation of the response function of the $LaBr_3$(Ce) detector to the gamma-ray beam. The result is shown by the red line in Fig. 11. One can see that the Geant4 simulation well reproduces the experimental response function (black line). Phenomenologically, as the scattering angle decreases in the slant-scattering, incident gamma-ray spectra of Gaussian function better fit the experimental response function in the Geant4 [30] simulation. In this phenomenological study, it was found that the energy resolution of 2 – 15 % can be obtained in the collimator aperture of 1 – 3 mm.

A thorough study of the energy resolution of the gamma-ray beam requires more realistic Geant4 simulations in which gamma-ray beams are kinematically produced in the laser Compton scattering, transported through the collimator system, and incident on the $LaBr_3$(Ce) detector. The energy distribution of the gamma-ray beam produced in the laser Compton scattering depends on the electron beam emittance, which is an important parameter to reproduce the experimental response function. A thorough analysis by means of more realistic Geant4 simulations will be done in the near future.

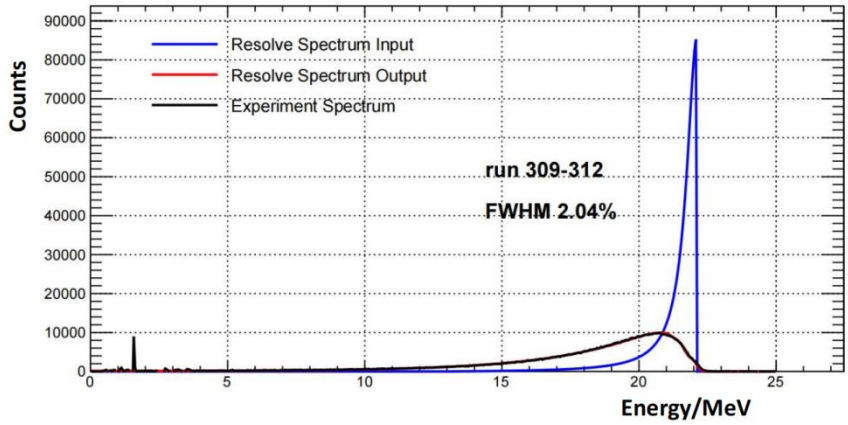

Fig. 11 Experimental response function of the $LaBr_3$(Ce) detector to a gamma-ray beam produce in the back- scattering at 180° (black line), a truncated Breit-Wigner function (blue line) assumed for the energy distribution of the gamma-ray beam, and a Geant4 simulation of the $LaBr_3$(Ce) response function (red line) to the gamma-ray beam (blue line).

4.5 Experimental spectrometers

We have developed four types of experimental spectrometers (sometime called as detector array) shown in Fig. 12, which are gamma nuclear resonance fluorescence (NRF) spectrometer(a), neutron flat-efficiency detector(FED) spectrometer (b), neutron time-of-flight (TOF) spectrometer(c) , and light charged-particles (LCP) spectrometer(d) . The four experimental spectrometers are used for the photon elastic/ inelastic scattering reaction, the photo-neutron reaction and the photo-light charged particle reaction, respectively. The spectrometer for photo-fission reaction is not involved in the current construction stage. The photonuclear reaction experiment can also employ a combination of two spectrometers, such as FED combined with NRF spectrometer will be used in (γ,nγ) experiment [31].

The NRF gamma spectrometer consists of two large-volume coaxial HPGe detectors, two clover HPGe detectors [32], and eight 3”(76.2 mm) x 4”(101.2 mm) $LaBr_3$(Ce) detectors [28]. The neutron FED consists of twenty-six ^{3}He counters [33] embedded in the polyethylene moderator [34]. The TOF neutron spectrometer consists of twenty Φ5”(127 mm) x 2”(50.8 mm) EJ301 [35] liquid scintillation detectors. The LCP (p,d,t,α) spectrometer consists of 4-6 groups ΔE-E telescope detectors composed of the grid ionization chamber (GIC) [36], silicon strip detector (SSD) [37] and CsI (Tl) crystal [36] mounted in a larger high-vacuum experimental chamber shown in Fig. 12 (d).

Fig.12. Four types of experimental spectrometers available in the SLEGS experimental station, gamma nuclear resonance fluorescence spectrometer (a), neutron Flat Efficiency detector spectrometer (b), neutron time-of-flight Spectrometer (c) and light charged particle spectrometer (d).

5. Results of the commissioning of the SLEGS beamline

The SLEGS beamline started the first test run at a small electron-beam current 10 mA in July 2021 and finished the debugging of the gamma-beam generation in back- and slanting-scattering modes at 200 mA. The performance of the SLEGS beamline in generating gamma-ray beams and the experimental spectrometer was approved by the Chinese Academy of Sciences (CAS) [38] in December 2021 and the construction of the SLEGS beamline station is completed. Results obtained in the commissioning run are summarized in Table 1.

Table 1. The commissioning results of SLEGS

Commissioning item		Final measured results
Beamline	Energy	0.25 - 21.7 MeV
	Resolution	~ 2-15 % (with collimator)
	Full-spectrum integrated gamma flux	~ 2.1 x 10^4 photons/s at 20° ~ 2.5 x 10^6 photons/s at 90° ~ 1.2 x 10^7 photons/s at 180° (for 300 mA e- and 5 W CO_2 laser)
	Angular divergence	< 0.45 mrad
Experimental Station	Charged particle Detector	Energy resolution <0.5 % at 5.5 MeV Position resolution ≤2 mm
	High efficiency gamma detector	Energy resolution <0.3 % at 662 keV Relative efficiency > 94 %

Table 2 shows the situation of several LCS facilities in the world and the comparison of main gamma parameters. Currently, only HIγS and SLEGS can provide MeV gamma rays for nuclear physics research.

Table 2. The current operation of Lase Compton Scattering (LCS) facilities in the world
(BCS-Back Compton scattering mode, SCS-Slant Compton scattering mode)

Facility/LCS Name	Collision Mode	Energy Range	Gamma Flux	Energy Resolution	current operating status
TUNL/HIγS (USA)	BCS	1-100MeV	10^{6-9} phs/s	(0.8-10)%	1996 -, open
SSRF/SLEGS (China)	BCS/SCS	0.25-21.7MeV	10^{5-8} phs/s	< 5%@2mm	2022 -, open
ELI-NP/VEGA (Europe)	BCS	0.2-19.5MeV	~ $2.5x10^{8}$ phs/s@10MeV	≤ 0.5@2mm	under construction
NewSUBARU/BL01(Japan)	BCS	1-76MeV	~ 10^{7} phs/s	~10%@3mm	2007 -, LCS, limited operation
UVSOR-III/BL01 (Japan)	BCS/SCS	1-5.4MeV	~ 10^{7} phs/s	~2.9%@2mm	2015 -, open
SPRing-8 /LEPS&LEPS2 (Japan)	BCS	1300-2900MeV	10^{6-7} phs/s	< 15%@tagging	1999 -, open

6. Summary and prospects

The completion of the SLEGS beamline station has been approved by the Chinese Academy of Sciences (CAS) in December 2021 through the successful commissioning run. Gamma-ray beams are produced in the energy range from 0.25 to 21.1 MeV in the laser Compton slant-scattering with 10.64 μm CO_2 laser photons at scattering angles from 20° to 160° , and at the maximum energy of 21.7 MeV in the laser Compton back-scattering at 180°. The slant-scattering mode is employed in the SLEGS beamline to systematically produce gamma-ray beams.

The two-stage coarse and fine collimators are used to produce fine pencil-like quasi-monochromatic gamma-ray beams. The gamma-ray integrated flux is 2.1 x 10^4 photons/s at 20°, 2.5 x 10^6 photons/s at 90° and 1.2 x 10^7 photons/s at 180°. The energy spread of the gamma-ray beam is 2 -15 % when the gamma-ray emission angle is confined less than 0.45 mrad at 38m with the collimator system. Four types of spectrometers, which may meet the versatility of nuclear physics experiments [39-44], are available in the SLEGS experimental station. The SLEGS beam line will be open to users by the end of 2022. In recent years, some large nuclear scientific facilities have started construction and put into operation, such as Back-streaming neutron(Back-n) source[45,46] at China Spallation Neutron Source(CSNS), High Intensity Heavy-ion Accelerator Facility (HIAF)[47-49] and CSR External-target Experiment(CEE) [50], Collinear Laser Spectroscopy (CLS)[51,52] and the new Beijing Radioactive Ion-beam Facility (BRIF) [53] etc., The completion of these facilities or devices will surely push China's nuclear physics basic and applied research to a new stage.

Acknowledgement

The authors thanks the SSRF leaders Zhao Zhentang (Academician), Tai Renzhong, and managers and chief engineers Li Aiguo, Leng Yongbin, Wang Jie, Huang Yuying, Xue Song, Zhang Wenzhi, Jiang Bocheng, Zhu Wanqian and other colleagues in the accelerator department and the beamline engineering department of SSRF for their technical support and assistance.

References

[1] Experimental Nuclear Reaction Data (EXFOR)， https://www-nds.iaea.org/exfor/exfor.htm

[2] IAEA TECDOC-1178, Handbook on Photonuclear Data for Applications Cross -sections and Spectra. Final report of a co-ordinated research project, (2000)，https://www.iaea.org/publications/6043/handbook-on-photonuclear-data-for-applications-cross-sections-and-spectra

[3] T.Kawano, Y.S.Cho, P.Dimitriou. et al., IAEA Photonuclear Data Library 2019, Nuclear Data Sheets, 163, 109-162 (2020), https://doi.org/10.1016/j.nds.2019.12.002

[4] V.V. Varlamov, Reliability of Photonuclear Data: Various Experiments and Evaluations. Phys. Part. Nuclei 50, 637-643 (2019). https://doi.org/10.1134/S1063779619050241

[5] V.V. Varlamov, A.I.Davydov, Physical Reliability Criteria and Special Features of Data on the Photodisintegration of ^{75}As, ^{127}I, ^{181}Ta, and ^{208}Pb, Nuclei. Phys. Atom. Nuclei 84, 603-614 (2021). https://doi.org/10.1134/S1063778821050148γ

[6] H.Ohgaki, H.Toyokawa, K.Yamada et al., Enchancement of Laser Compton gamma-ray beam with F-P cavity in storage ring TERAS, Free Electron Lasers 2003, Proceedings of the 25th International Free Electron Laser Conference and the 10th FEL Users Workshop, Tsukuba, Ibaraki, Japan, 8-12 September (2003), https://doi.org/10.1016/B978-0-444-51727-2.50143-7

[7] NewSUBARU BL01, Laser Compton Gamma Source, https://www.lasti.u-hyogo.ac.jp/NS-en/facility/bl01/

[8] High Intensity Gamma-Ray Source (HIGS), https://tunl.duke.edu/research/our-facilities

[9] A. M. Sandorfi, M. J. LeVine, C. E. Thorn, et al., High Energy Gamma Ray Beams from Compton Backscattered Laser Light, IEEE Transactions on Nuclear Science, 30, 3083-3087, (1983), https://doi: 10.1109/TNS.1983.4336577.

[10] LEPS-Laser Electron Photon Experiment at SPring-8, https://www.rcnp.osaka-u.ac.jp/Divisions/np1-b

[11] Extreme Light Infrastructure - Nuclear Physics (ELI-NP), www.eli-np.ro

[12] X. Z. Cai, J. H. Gu, W. Guo, et al., Research on properties and application of Compton backscattered gamma light source based on synchrotron radiation accelerator, Progress in Physics, 23, 389, (2003), https://doi:10.3321/j.issn:1000-0542.2003.04.001 (in Chinese)

[13] W. Guo, W.Xu, J.G.Chen et al., A high intensity beam line of γ-rays up to 22 MeV energy based on Compton backscattering, Nucl. Instr. and Meth. A 578 , 457 (2007), https://doi.org/10.1016/j.nima.2007.05.322

[14] J.G. Chen, W. Xu, W. Guo et al., An X-ray source based on Compton backscattering of CO_2 laser and 100 MeV electrons, Nucl. Instr. and Meth. A 580, 1184-1190 (2007) , https://doi.org/10.1016/j.nima.2007.07.007

[15] W. Luo, W. Xu, Q.Y. Pan et al., Laser Compton scattering experiments and the latest developments in construction of experimental facilities at SINAP, Proc. SPIE, V7385, 73852D (2009), DOI: 10.1117/12.835572

[16] W. Luo, W. Xu, Q.Y. Pan et al., A laser-Compton scattering (LCS) prototype experiment at 100MeV Linac of Shanghai Institute of Applied Physics, Rev. of Sci. Instr., 81, 013304 (2010), https://doi:10.1063/1.3282445.

[17] W. Luo, W. Xu, Q.Y. Pan et al., An X-ray spectroscopy system and its application to the Laser-Compton scattering experiments, Nucl. Instr. and Meth. A 624,141-147 (2010) , https://doi:10.1016/j.nima.2010.09.045

[18] W.Luo, W.Xu, Q.Y.Pan et al., A 4D Monte Carlo laser-Compton scattering simulation code for the characterization of the future energy-tunable SLEGS, Nucl. Instr. and Meth. A660, 108-115(2011), https://doi.org/10.1016/j.nima.2011.09.035

[19] W. Luo, W. Xu, Q.Y. Pan et al., X-ray generation from slanting laser-Compton scattering for future energy-tunable Shanghai Laser Electron Gamma Source, Applied Physics B, 101, 761-771 (2010), https://doi.org/10.1007/s00340-010-4100-0

[20] H.W. Wang, G.T. Fan, L.X. Liu et al., Development and Prospect of Shanghai Laser Compton Scattering Gamma Source. Nucl. Phys. Rev., 37(1), 53-63 (2020). https://doi:10.11804/NuclPhysRev.37.2019043 (in Chinese)

[21] Y. Taira, M.Adachi, H.Zen, et al., Generation of Ultra-Short Gamma Ray Pulses via Laser Compton Scattering in UVSOR-II Electron Storage Ring, in International Conference on Ultrafast Phenomena, OSA Technical Digest (CD) (Optica Publishing Group), paper TuE22, (2010) https://opg.optica.org/abstract.cfm?URI=UP-2010-TuE22

[22] Y. Taira, M. Adachi, H. Zen et al., Generation of energy-tunable and ultra-short-pulse gamma rays via inverse Compton scattering in an electron storage ring, Nucl. Instr. And Meth. A 652, 696-700 (2011). http://dx.doi.org/10.1016/j.nima.2010.08.036

[23] H. H. Xu, G. T. Fan, H.W. Wang et al., Interaction chamber for laser Compton slant scattering in SLEGS beamline at Shanghai Light Source, Nucl. Instr. and Meth, Phys. A 1033, 166742 (2022); published online (https://doi.org/10.1016/j.nima.2022.166742).

[24] Z.R.Hao, G.T.Fan, H.W.Wang, et al., Collimator system of SLEGS beamline at SSRF, Nucl. Instr. and Meth. A,1013, 165638 (2021), https://doi.org/10.1016/j.nima.2021.165638

[25] Z.R.Hao, G.T.Fan, H.W.Wang, et al., A new annular collimator system of SLEGS beamline at SSRF, Nucl. Instr. and Meth. B, 519,9-14, (2022) , https://doi.org/10.1016/j.nimb.2022.02.010

[26] COHERENT, https://www.coherent.com/

[27] Saint-Gobain, https://www.crystals.saint-gobain.com

[28] ADVACAM, https://advacam.com/minipix

[29] SICCAS, http://www.siccas.com/

[30] Geant4, https://geant4.web.cern.ch/

[31] H. Utsunomiya, Z.R. Hao, S. Goriely et al., p-process chaser detector in - coincidences, Nucl. Instrum. Methods, Phys. Res. A 1034, 166819 (2022), https://doi.org/10.1016/j.nima.2022.166819.

[32] Canberra, https://www.mirion.com/

[33] LND, https://www.lndinc.com/about/

[34] Z.R. Hao, G.T. Fan, L.X. Liu et al., Design and simulation of 4π flat-efficiency ^{3}He neutron detector array, Nucl. Tech., 43, 57-65(2020), DOI: 10.11889/j.0253-3219.2020.hjs.43.110501(in Chinese)

[35] ELJEN, https://eljentechnology.com/

[36] Institute of Modern Physics, CAS, www.impcas.ac.cn

[37] Micron Semiconductor, www.micronsemiconductor.co.uk

[38] Chinese Academy of Science(CAS), http://www.cas.ac.cn/
[39] H. Utsunomiya, T. Shima, K. Takahisa et al., Energy Calibration of the NewSUBARU Storage Ring for Laser Compton-Scattering Gamma Rays and Applications, IEEE Trans. On Nucl. Sci, 61, 1252-1258 (2014), https://doi:10.1109/TNS.2014.2312323
[40] Y. Xu, W. Xu, Y. G. Ma et al., Determination of the Stellar Reaction Rate for $^{12}C(\alpha,\gamma)\ ^{16}O$:Using a New Expression with the Reaction Mechanism, Chin. Phys. B, 18, 1421-1407 (2009), https://doi:10.1088/1674-1056/18/4/023.
[41] Y.J. Li, W. Xu, W. M. Snow et al., Measurement of PV asymmetry in n + p→d + γ and γ+ d→n + p, Chin. Phys. C 34, 1465 (2010) ,https://doi.org/10.1088/1674-1137/34/9/073.
[42] Z.D. An, Y.G. Ma, G.T. Fan et al., New Astrophysical Reaction Rate for the $^{12}C(\alpha,\gamma)^{16}O$ Reaction, The Astr. Jour. Lett. 817, L5 (2016), https://doi.org/10.3847/2041-8205/817/1/L5.
[43] Z.R Hao, G.T. Fan, L.X. Liu et al., Design and simulation of 4π flat-efficiency ^{3}He neutron detector array. Nucl. Tech., 43, 110501(2019)， https://doi:10.11889/j.0253-3219.2020.hjs.43.110501(in Chinese)
[44] J.W. Wang, G.T. Fan, H.W. Wang et al., Study on polarized γ beam properties of a new LCS light source based on SXFEL. Nucl. Tech., 42,120201(2019). https://doi:10.11889/j.0253-3219.2019.hjs.42.120201(in Chinese)
[45] J.Y. Tang, Q. An, J.B. Bai, et al. Back-n white neutron source at CSNS and its applications. Nucl. Sci. Tech. 32, 11 (2021). https://doi.org/10.1007/s41365-021-00846-6
[46] X.R. Hu, G.T. Fan, W. Jiang, et al. Measurements of the $^{197}Au(n, \gamma)$ cross section up to 100 keV at the CSNS Back-n facility. Nucl. Sci. Tech. 32, 101 (2021). https://doi.org/10.1007/s41365-021-00931-w
[47] X.F. Niu, F. Bai, X.J. Wang, et al. Cryogenic system design for HIAF iLinac. Nucl. Sci. Tech. 30, 178 (2019). https://doi.org/10.1007/s41365-019-0700-5
[48] J.H. Liu, Z. Ge, Q. Wang, et al. Electrostatic-lenses position-sensitive TOF MCP detector for beam diagnostics and new scheme for mass measurements at HIAF. Nucl. Sci. Tech. 30, 152 (2019). https://doi.org/10.1007/s41365-019-0676-1
[49] M.T. Tang, L.J. Mao, H.J. Lu, et al. Design of an efficient collector for the HIAF electron cooling system. Nucl. Sci. Tech. 32, 116 (2021). https://doi.org/10.1007/s41365-021-00949-0
[50] L.M. Lyu, H. Yi, L.M. Duan et al. Simulation and prototype testing of multi-wire drift chamber arrays for the CEE. Nucl. Sci. Tech 31, 11 (2020). https://doi.org/10.1007/s41365-019-0716-x
[51] S.W. Bai, X.F. Yang, S.J. Wang et. al., Commissioning of a high-resolution collinear laser spectroscopy apparatus with a laser ablation ion source, Nucl. Sci. Tech. 33, 9 (2022), https://doi.org/10.1007/s41365-022-00992-5
[52] S.J.Wang, X.F.Yang, S.W.Bai et al., Construction and commissioning of the collinear laser spectroscopy system at BRIF, Nucl. Instr. and Meth, Phys. A 1032, 166622(2022), https://doi.org/10.1016/j.nima.2022.166622
[53] W. Nan, B. Guo, C.J. Lin et al. First proof-of-principle experiment with the post-accelerated isotope separator on-line beam at BRIF: measurement of the angular distribution of $^{23}Na + ^{40}Ca$ elastic scattering. Nucl. Sci. Tech. 32, 53 (2021). https://doi.org/10.1007/s41365-021-00889-9